**Tidal modulation of ice streams: Effect of periodic sliding velocity on ice friction and healing**

**Christine McCarthy[1*], Rob M. Skarbek[1], Heather M. Savage[2]**

[1]Rock and Ice Mechanics Lab, Lamont-Doherty Earth Observatory, Columbia University, New York, NY USA

[2]Earth & Planetary Sciences, U.C. Santa Cruz, Santa Cruz, CA USA

*** Correspondence:**
Christine McCarthy
mccarthy@ldeo.columbia.edu

**Keywords: tidal modulation[1], ice friction[2], basal sliding[3], stability[4], healing[5]. (Min.5-Max. 8)**

**Abstract**

Basal slip along glaciers and ice streams can be significantly modified by external time-dependent forcing, although it is not clear why some systems are more sensitive to tidal stresses. We have conducted a series of laboratory experiments to explore the effect of time varying load point velocity on ice-on-rock friction. Varying the load point velocity induces shear stress forcing, making this an analogous simulation of aspects of ice stream tidal modulation. Ambient pressure, double-direct shear experiments were conducted in a cryogenic servo-controlled biaxial deformation apparatus at temperatures between -2°C and -16°C. In addition to a background, median velocity (1 and 10 μm/s), a sinusoidal velocity was applied to the central sliding sample over a range of periods and amplitudes. Normal stress was held constant over each run (0.1, 0.5 or 1 MPa) and the shear stress was measured. Over the range of parameters studied, the full spectrum of slip behavior from creeping to slow-slip to stick-slip was observed, similar to the diversity of sliding styles observed in Antarctic and Greenland ice streams. Under conditions in which the amplitude of oscillation is equal to the median velocity, significant healing occurs as velocity approaches zero, causing a high-amplitude change in friction. The amplitude of the event increases with increasing period (i.e. hold time). At high normal stress, velocity oscillations force an otherwise stable system to behave unstably, with consistently-timed events during every cycle. Rate-state friction parameters determined from velocity steps show that the ice-rock interface is velocity strengthening. A companion paper describes a method of analyzing the oscillatory data directly. Forward modeling of a sinusoidally-driven slider block, using rate-and-state dependent friction formulation and experimentally derived parameters, successfully predicts the experimental output in all but a few cases.

## 1 Introduction

Ice streams represent a significant portion of the Antarctic ice mass balance [e.g., *Bamber et al.,* 2000]. Much of the dynamics that control ice stream flow rates are not well constrained, particularly sliding at the base. Modeling efforts often consider local variation and evolution of basal resistance as a control on flow rates [e.g. *Clarke*, 2005]. However, our knowledge of the base is limited to but a few locations. Meanwhile, a growing body of literature documents the sensitivity of ice stream flow to tidal forcing [*Riedel et al*., 1999; *Doake et al*., 2002; *Bindschadler et al*., 2002; 2003; *Gudmundsson*, 2007; *Brunt et al.,* 2010; *Wuite et al*., 2009; *Rosier et al*., 2014; 2017], with modulation measured up to 100 km upstream from the grounding line [e.g. *Anandakrishnan and*

*Alley*, 1997]. Ice stream tidal modulation displays great variations in the type and periodicity of modulation. For instance, Mercer and Bindschlader Ice Streams display smooth, diurnal modulation [*Brunt and MacAyeal*, 2014; *Anandakrishnan et al*, 2003] whereas Rutford Ice Stream's smooth modulation is semi-diurnal and more closely tuned to the spring-neap cycle [*Murray et al*., 2007; *Minchew et al.*, 2017]. Long period modulation provides changes in horizontal flow velocities in the range of 5% to 20% of the mean velocity, whereas the short period modulations have given rise to ~300% the mean velocity, in some cases causing periodic reversal in flow direction [*Makinson et al*., 2012]. Whillans Ice Stream is a noteworthy example in which the tidal modulation is in the form of stick-slip, captured by both GPS and seismic records [e.g. *Weins et al*., 2008; *Winberry et al.,* 2009, 2011; 2014; *Pratt et al*., 2014; *Barcheck et al*., 2021] in which bursts of motion are followed by long periods of near stagnation. The twice-daily 30 min events occur just before low tide and just after high tide [*Wiens et al., 2008*]. The relationship between displacement during an event and recurrence interval suggests a time-dependent strengthening, or healing, at the basal interface between events [*Winberry et al.,* 2014]. Variations in modulation style and tuning from location to location raise the possibility of using glacier response to relatively well-known tidal signals to infer basal properties.

The effects of periodic perturbations on frictional stability has been studied in laboratory experiments on both solid and granular materials, with oscillations in shear forcing [*Lockner and Beeler*, 1995; *Savage and Marone*, 2007; 2008], oscillations in normal stress forcing [*Richardson and Marone,* 1999; *Boettcher and Marone*, 2004; *Hong and Marone*, 2005], and oscillations in principal stresses [*Beeler and Lockner*, 2003]. The effects of periodic perturbations have additionally been reviewed in theoretical treatments [*Tworzydlo and Hamzeh*, 1997; *Voisin*, 2001, 2002; *Perfettini and Schmittbuhl*, 2001; *Perfettini et al.,* 2003]. These studies have provided insight into frictional modulation and dynamic triggering of stick-slip, including the frequency- and amplitude-dependences of rock and gouge systems.

In an attempt to provide physical mechanisms responsible for differing sliding behaviors and aid in prediction of future flow rates, we run a series of cyclically forced friction experiments to explore the onset of stick-slip and slow slip in a simple ice-on-rock system. We explore the effects of temperature, period, amplitude, normal stress, and velocity on the frictional strength and stability. We apply the mathematical framework of rate-and-state friction with an analysis of velocity steps to describe the laboratory results and forward model the behavior with a simple 1D slider block model to determine if the observed behavior is consistent with existing theory.

## 2 Materials and Methods

Rectangular samples of polycrystalline ice were fabricated using a modified version of the "standard ice" protocol [*Cole*, 1979; *McCarthy et al*., 2017], which used seed ice that was shaved, sieved (between 250 and 106 mm), and packed into a rectangular mold. The mold was placed in an ice bath (T = 0°C) for ~30 mins, under vacuum. Upon temperature equilibration, the mold was flooded with degassed deionized water and then placed on a cold copper plate (T = -5°C) within a chest freezer, insulated on all sides, to allow directional solidification from the bottom up. The resulting samples were nearly pore-free (<1%) with uniform grain size of approximately 1 mm (due to subsequent grain growth at the relatively warm -5°C). Samples were made intentionally oversized; after removal from the mold, they were cut down to precise dimensions (50x50x100mm) with a microtome located in a cold room (T = -17°C). The ice sliding surfaces were roughened with 100 grit sandpaper just before loading into the apparatus.

Experiments were conducted in a double-direct shear configuration (Fig. 1 Inset) using an ambient pressure, servo-controlled biaxial apparatus [*McCarthy et al.*, 2016]. Experiments were conducted over a range of temperatures that were controlled via a circulating fluid cryostat (-2 < T(°C) < -16). In the experiments, the central polycrystalline ice block (50x50x100mm) was slid between two stationary blocks of Barre granite (50x50x30mm) such that the nominal area of contact (50x50 on each of two sliding faces) was constant during sliding. A horizontal piston pushing against a screw stop applied constant normal stress that was maintained using force feedback servo control. Shear stress was induced by a vertical ram that was servo-controlled in displacement feedback using a computer-controlled driving program. The force applied and the displacement travelled in each direction were measured by load cells and displacement transducers, respectively, mounted outside the cryostat. The stiffness of the apparatus and sample assembly is 0.46±0.29 kPa/μm, as determined *in situ* by measuring shear stress vs. displacement curves.

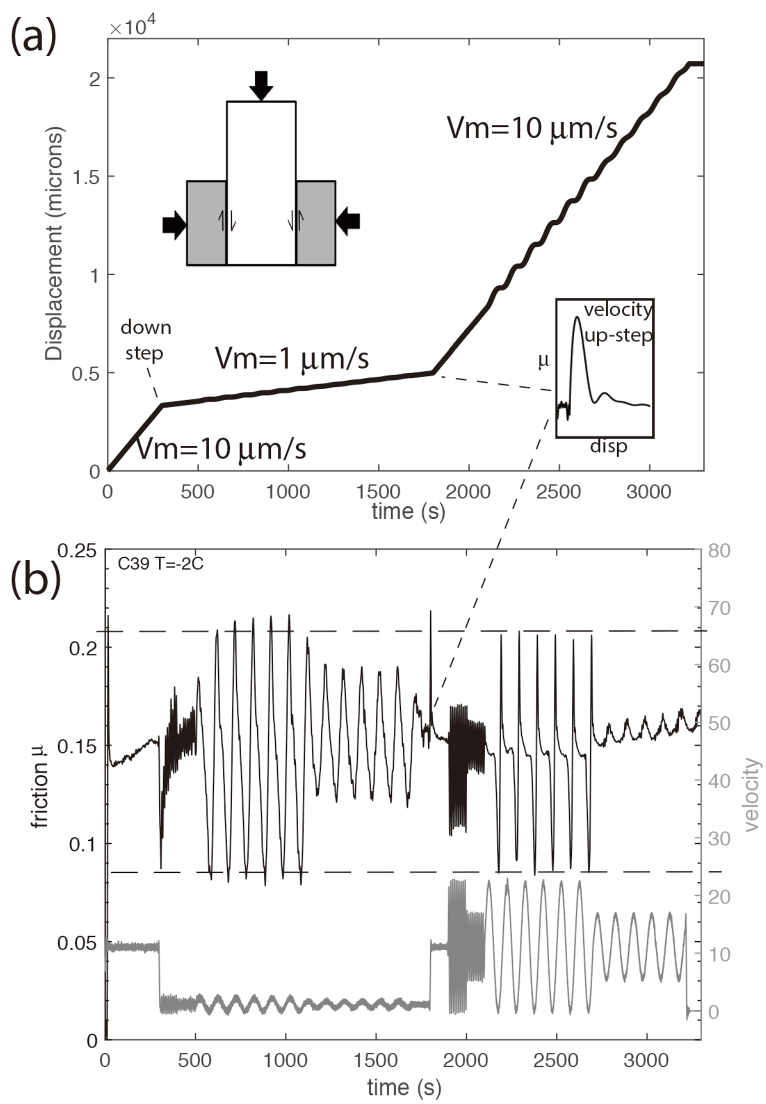


**Figure 1:** (a) Displacement vs. time showing the driving control program. (b) Driving velocity in gray and measured friction (black) for a single run of ice sliding on rock in double direct shear (upper inset) at -2°C.

We combined a constant load point velocity with sinusoidal oscillations (Fig. 1a). In every experiment, a constant velocity was first applied for approximately 3 mm of displacement to precondition the sample such that steady-state friction was reached. After that, multiple amplitudes and periods were applied in succession (from short to long) to study the frictional response (Table 1). The load point was moving at *V(t),* which we describe as a function of forcing period *P* and amplitude *A* as:

$$V(t) = V_m + A\cos\left(\frac{2\pi t}{P}\right). \quad (1)$$

Specifically, two different driving protocols were used. Experiments C28 to C33 used a single median driving velocity ($V_m$ = 10 μm/s) and cycled through three periods (1, 10, and 100 s) with three amplitudes each (10, 5, and 2 μm/s, which are 100%, 50%, and 20% of $V_m$), such that at the highest amplitude velocities slowed to zero once per cycle, but the sample never moved backward. Experiments C31 and C33 further explored 5 and 50 s periods. Experiments C34 to C44 tested only two periods (10 and 100 s) and two amplitudes (100% and 50% of $V_m$) but employed two median driving velocities (1 and 10 μm/s) such that a full set of oscillations were conducted at 1 μm/s, the velocity was increased to 10 μm/s, and another full set of oscillations were repeated (Fig. 1). The transition between the two rates represents a velocity upstep (Fig. 1a inset), which was used to measure rate-state parameters described in Eqs. 2–4. During most experiments, a constant normal stress of ~0.1 MPa was applied, with the exception of C41 and C44, during which we first ran the two-velocity cycling program under 0.5 MPa normal stress and then repeated the program under 1 MPa normal stress. In total, 10 samples were tested with runs covering 107 different combinations of $V_m$, *T*, *P*, and *A* conditions. Some conditions were additionally repeated to confirm reproducibility, as discussed in Section 4.5 and in the supplementary material.

Temperature during an experiment was held constant with a circulating fluid- controlled cryostat described in *McCarthy et al*., 2016; 2017. However, several improvements were incorporated into the temperature control and monitoring system since those previous works. A resistance temperature detector (RTD) embedded in the rock monitored temperature at the sliding interface between ice and rock. The RTD has an error of ±0.1°C, which was a significant improvement over the previously used thermocouples. Additionally, here the bottom plate of the cryostat was made of insulating material (polycarbonate) so that external heating did not transfer to the stationary steel blocks holding the rock samples. Finally, we pre-chilled all rock and metal in the cryostat overnight at the desired testing temperature before each experiment. These three changes created a system that achieved and held a desired temperature more efficiently than our previous cryostat.

## 3 Inversion for Rate and State Friction Parameters and Forward modeling

Variations between smooth (stable) sliding and stick-slip (unstable) sliding in cyclically forced ice friction experiments can be modeled using rate-and-state friction, an empirical characterization of frictional strength as a function of both sliding velocity *V* (the relative slip rate across a contact interface) and state θ (which at steady state is the lifetime of asperity contact) that has been successfully used in rock mechanics to describe earthquake phenomena for decades [e.g. *Dieterich*, 1979, 1981; *Ruina*, 1983], and has more recently been employed to describe sliding behavior in Antarctic Ice Streams [e.g. *Zoet et al*., 2013; *Lipovsky and Dunham*, 2017; *Lipovsky et al*., 2019]. In the formulation, rate and state are related by coupled equations, the first of which is the friction law:

$$\mu(V,\theta)=\frac{\tau}{\sigma_n}=\mu_0+a\ln\frac{V}{V_0}+b\ln\frac{V_0\theta}{D_C}, \tag{2}$$

in which τ and $\sigma_n$ are shear and normal stresses, respectively, $a$ is the "direct effect" accounting for variations in frictional strength due to changes in slip rate from a reference velocity, $b$ is the "evolution effect" that determines the change in friction due to evolution of state from a reference steady state, and $D_c$ is the critical slip distance that is needed for the system to evolve from one steady-state to another [*Dieterich, 1979; Marone, 1998*]. Parameters $a$, $b$, and $D_c$ are determined from experimental velocity step data (Fig. 1inset) and $\mu_0$, $V_0$, and $\theta_0$ are reference values such that $\mu(V_0, \theta_0) = \mu_0$. The two forms of the time evolution of state are:

$$\dot{\theta}=1-\frac{V\theta}{D_C}\text{, the Aging Law [\textit{Dieterich}, 1978]} \tag{3}$$

and

$$\dot{\theta}=-\frac{V\theta}{D_C}\ln\frac{V\theta}{D_C}\text{, the Slip Law [\textit{Ruina}, 1983].} \tag{4}$$

The Aging law and Slip Law are similar in that at steady state sliding, both are $V\theta/D_c= 1$. They differ in that the Aging law describes state evolution during stationary contact while the Slip Law describes state changing only during slip. Hooke's law applied to a single-degree-of -freedom spring slider is used to approximate the elastic response of the apparatus (and sample), which, combined with the rate and state friction equations, allows experimental data to be analyzed. In terms of velocity and the friction coefficient, the relation is:

$$\frac{\partial\mu}{\partial t}=k(V_L-V) \tag{5}$$

where $k$ is the elastic stiffness with units 1/length.

Previous experimental studies introduced a critical forcing period of the oscillating velocity, which determines the stability transition of the system. There are two timescales that have been proposed to govern the response of sliding to a given frequency. One is the natural period of the spring-slider system, which is proportional to the critical slip distance $D_c$ and load point velocity $V$ as [*Rice and Ruina*, 1983; *Boettcher and Marone*, 2004; *Savage and Marone*, 2007; *van der Elst and Savage*, 2015]:

$$P_C\propto\frac{D_C}{V} \tag{6}$$

The nucleation timescale describes the time from the initiation to fully unstable slip [*Dieterich*, 1994; *Beeler and Lockner*, 2003; *van der Elst and Savage*, 2015]:

$$P_n=\frac{a\sigma_n}{\dot{\tau}} \tag{7}$$

where $\dot{\tau}$ is the load point velocity multiplied by the system stiffness *k,* which includes the stiffness of the apparatus and the sample. Critical stiffness is defined as:

$$k_C = \frac{\sigma_n(b-a)}{D_C} \tag{8}$$

such that steady, stable sliding occurs when the system stiffness exceeds critical stiffness $k > k_c$ [*Rice and Ruina*, 1983; *Gomberg et al*., 1997]. Stable sliding corresponds to creeping, or smoothly sliding, and is associated with rate-strengthening friction ($a$-$b \geq 0$). Sliding is conditionally stable when the system is rate-weakening ($a$-$b < 0$) and is the necessary condition for stick-slip behavior [e.g., *Scholz*, 2002]. Stress decreases during a sliding event, and thus healing is also needed to facilitate strength recovery for repeated slip events [e.g., *Carpenter et al*., 2011]

Velocity up-steps from raw data were analyzed with a nonlinear least squares fitting routine to a spring slider with stiffness *k*. In the fitting GUI (RSFit3000), slider velocity, friction coefficient (Eq. 2), and both Eqs. 3 (Aging) and 4 (Slip) descriptions of state are cast as coupled ordinary differential equations (ODEs) [*Skarbek and Savage,* 2019]. Although recent studies have shown that the Slip law does a better job of describing experimental data [*Bhattacharya et al.* 2015; 2017], we provide fits for both for comparison. A single state variable was used and the fitting program minimizes the difference between the data for steady-state friction, *a*, *b*, and $D_c$ user inputs for initial guesses. The standard deviation of the *(a-b)* combined parameter in the GUI is computed using the covariance between *a* and *b* [*Skarbek and Savage*, 2019; their Eq. 7]. Since we anticipate that system stiffness depends on changes in state as predicted by the spring- slider system, we additionally solved for *k*. For more discussion of this and for additional details about the RSFit3000 fitting GUI, see *Skarbek and Savage, 2019*. Finally, a weighting function was included to ensure that the weight vector takes on values greater than unity at the velocity step and decays exponentially with load point displacement [*Reinen and Weeks*, 1993; *Blanpied et al*., 1998].

A forward model was created that uses a 1D elastic slider block (Eq. 5) and Eqs. (2) and (8) with sinusoidal load point velocity of Eq. (1) and the individual fitted parameters provided in Table 2 to predict the frictional response of the system at desired periods and amplitudes. Inertia is ignored in the model, such that the slider block is considered rigid. The forward model can employ either the Aging or Slip forms of state, but here we use Aging. The governing equations for state variable, friction coefficient, and slip velocity are cast as coupled ODEs.

## 4 Results

The results from these periodic forcing experiments, the first conducted in our apparatus, demonstrate first and foremost that by simply changing the frequency and amplitude of forcing, the full range of frictional behavior can be observed within a single experiment (Fig. 2). At small forcing amplitudes (20% of $V_m$) at longest and shortest periods, we see no discernible modulation of the friction coefficient (Fig. 2a) and erratic oscillation that cannot keep up with the forcing (Fig. 3a), respectively. For many conditions, particularly at long period, the response to a sinusoidal driving velocity is an in-phase sinusoid in friction (left side of Fig. 2d). At the longest period (100 s) a high amplitude event during each cycle is observed in the frictional response (Fig. 2d). For this event and the transitional stage in Fig. 2c, the maxima are not exactly in phase with the forcing. Rather, the minima occur just after the low velocity and the maxima just before the high velocity, so the response is always within the increasing velocity leg of the cycle. Starting from the median point in velocity and continuing with decreasing velocity, friction begins to relax. Just after velocity increases above zero (t1), friction responds rapidly to a peak value (at t2) then rapidly evolves back to the background oscillation value. This slow slip event thus resembles a slide-hold-slide superimposed on a sinusoid (to be discussed further in Sections 4.2 and the discussion). At some conditions slipping events occur twice per cycle (Fig. 2e) and at yet other conditions (high amplitude, high normal stress), audible stick-slips occur with significant stress drops, sometimes skipping cycles (period doubling; Fig. 2f). Herein we quantify specific effects related to systematically changing temperature, amplitude, normal stress, and median forcing velocity.

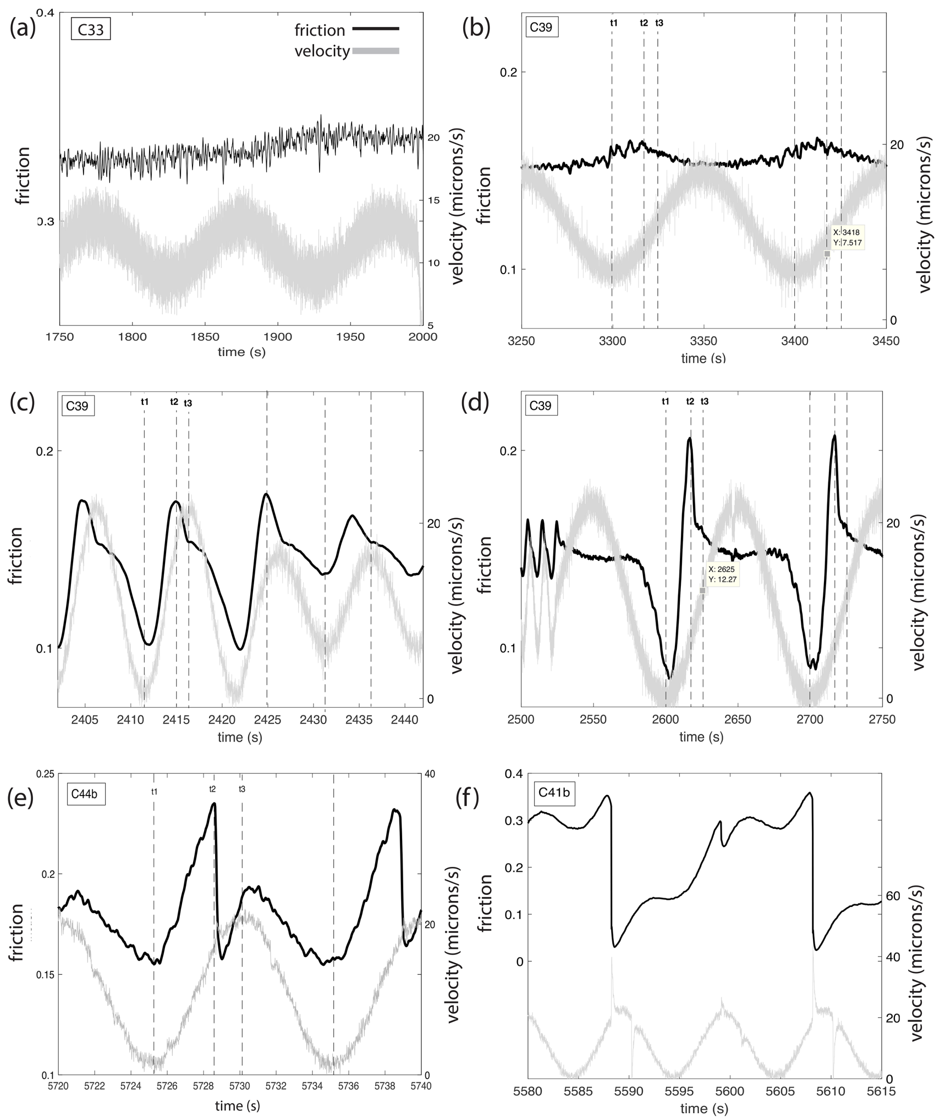


**Figure 2:** examples and magnification of different responses observed in the experiments: (a) at long period and small amplitude (20% of $V_m$) there is no modulation; (b) at long period at 50% of $V_m$ response is slight, with small uptick in friction occurring between the low velocity point (t1) and peak acceleration (t3); (c) at shorter period (10s) both 100% $V_m$ and 50% $V_m$ are modulated, but not with a simple sine wave; (d) a high amplitude event or slow slip event, which resembles a relaxation hold superimposed on a sine wave; (d) a double event (one fast, one slow) within a single cycle; (e) pronounced stick-slip events, with almost total stress drop, occurring every other cycle (period doubling) at 1 sec before maximum velocity.

### 4.1 Temperature effects

Under the range of conditions explored here, in which homologous temperatures $T/T_m$ were quite high, the primary effect of temperature was a decrease in the mean friction value. The average values are consistent with steady-state friction reported in a previous study [*McCarthy et al.*, 2017], in which samples were prepared identically, but were tested under constant load point velocities instead of oscillations. The one exception is the lowest temperature measured in this study, which deviates from the previous linear temperature dependence. Based on other studies of ice-on-ice friction, we do not anticipate the linearity to increase indefinitely. At approximately 0.75 $T/T_m$ (-70°C) friction of ice flattens to between μ = 0.6–0.9 without strong temperature dependence at homologous temperatures lower than that [e.g. *Schulson and Fortt*, 2012]. It is not clear if the discrepancy in Fig. 3d at T= -16°C is a reduction of friction due to oscillations or is just due to uncertainty in measuring temperature in our previous study (which used thermocouples).

Apart from this control on average friction, temperature effects on the frictional response are negligible at low normal stress (Figure 3). There is no temperature dependence on the amplitude of shear stress oscillations (Fig. 3b and 3c) and, as shown in sections 4.2 and 4.4, no discernable temperature dependence of healing or rate dependence (*a-b*) behavior, respectively. There is also no discernable effect of temperature on individual rate-state parameters (Table 2) within this admittedly narrow range of temperatures.

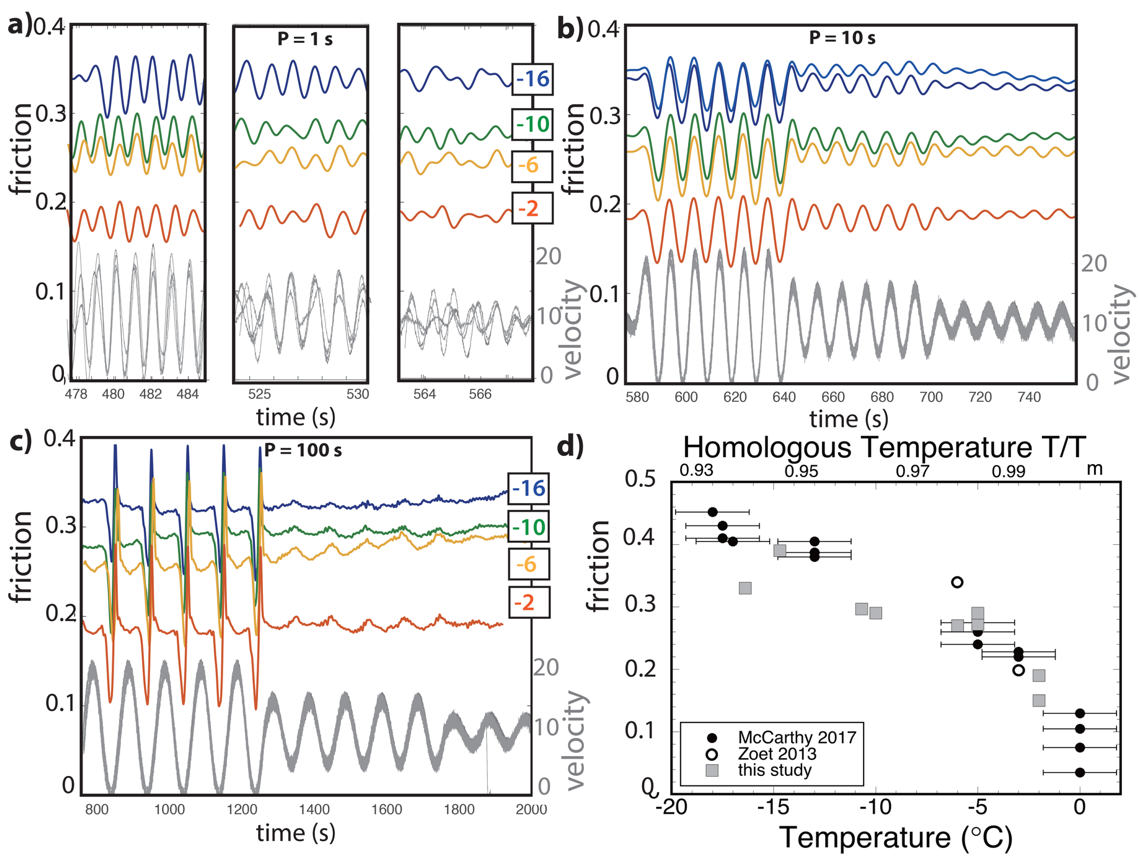


**Figure 3:** frictional response to periodic load point velocity (gray) as a function of temperature, at (a) 1 second periods; (b) 10 second periods; and (c) 100 second periods. (d) Temperature directly affects the average friction, consistent with steady state friction coefficients from previous studies [*Zoet et al., 2013*; *McCarthy et al., 2017*].

### 4.2 Amplitude and Period effects

Due to the similarity in form to slide-hold-slides, we measured the mid-to-peak amplitude of the oscillatory friction data (those that approach and reach zero velocity) (Fig. 4 inset). Although the peak level of friction upon reloading is more rounded than in typical slide-hold-slides, we use the maximum value during the cycle. The midpoint is determined by drawing a straight line from the steady state friction values before and after the oscillations. As shown in Fig. 4, the mid-to-peak amplitude of the oscillatory response is clearly a function of the period of forcing. The response resembles, in both magnitude and in slope, frictional strengthening determined from slide-hold-slide experiments in a previous study [*McCarthy et al.*, 2017]. A plot of amplitude vs. temperature provided in the Supplementary Material demonstrates no clear temperature dependence on the amplitude of the frictional response.

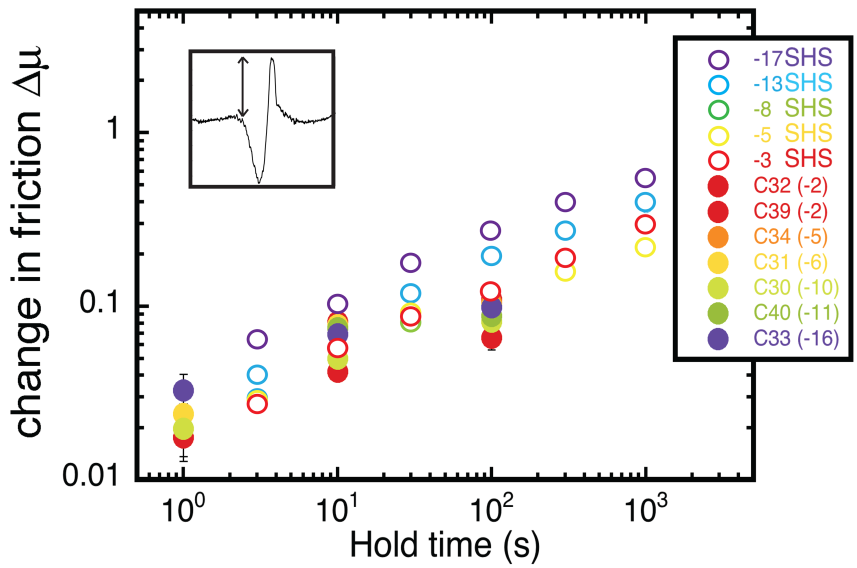


**Figure 4:** (a) frictional amplitude (inset) vs. period of forcing from this study (closed symbols) compared to delta friction and log hold time from previous slide-hold-slide experiments (open symbols) [*McCarthy et al, 2017*]

### 4.3 Normal stress effects

In Figs. 5 and 6 we document sliding behavior over a range of normal stresses (0.1 – 1 MPa) at T = -2°C (Fig. 5) and -5°C (Fig. 6). Shear stress increases linearly with normal stress at both of these temperatures (insets), consistent with Coulomb behavior. At lowest normal stress (0.1 MPa) for both temperatures, smooth sliding is observed under most forcings, similar to the data in Fig. 3. However, at elevated normal stresses of 0.5 and 1 MPa the data show sudden stress drops that were accompanied by audible pops during the experiment. In Fig. 6b, the response at $\sigma_n$ = 1 MPa demonstrates an event every other cycle (i.e. period doubling), with almost complete stress release during each event. These are stick-slips that occur ~1 sec before peak velocity (Fig. 2f). The events cause the piston and sample to jolt forward at almost 40 μm/s (double the programmed rate). Both the 0.5 and 1 MPa normal stress datasets also show a smaller event at the low velocity point. The audible high velocity events are analogous to earthquakes or stick slip events in glaciers.

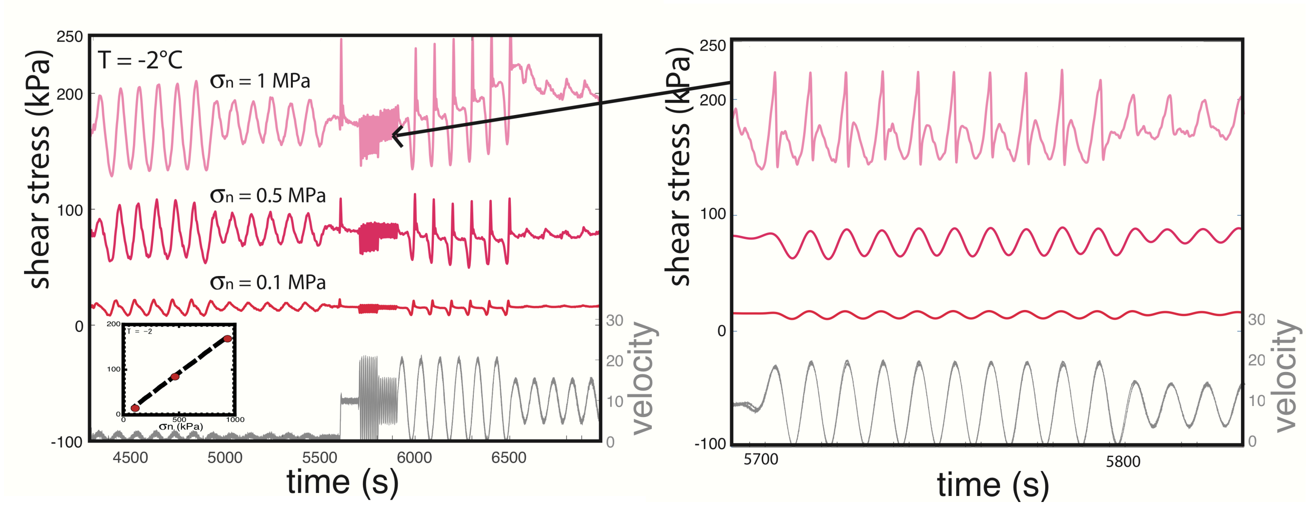


**Figure 5:** Shear stress response to periodic velocity as a function of normal stress, at T = -2°C. The responses display Coulomb friction (inset). At increasing normal stress, stick-slips are observed at 10 s period.

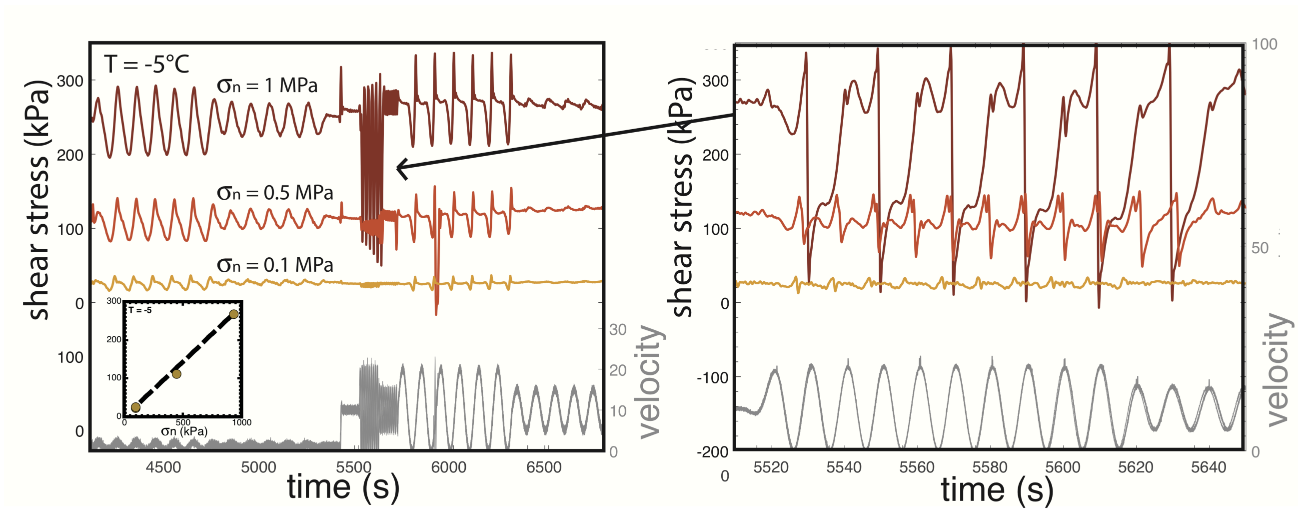


**Figure 6:** Shear stress response to periodic velocity as a function of normal stress, at T = -5°C. The responses display Coulomb friction (inset). At increasing normal stress, stick-slips and period doubling are observed

## 4.4 Velocity effects

During experiments C34 – C44, we employed a positive step in load point velocity from 1 μm /s to 10 μm /s at approximately the halfway point of the experiment (Fig. 1 inset). Using a least-squares inversion [*Skarbek and Savage*, 2019], we fit Eq. (2) and both the Aging (Eq. 3) and Slip (Eq. 4) forms of state evolution to the velocity steps (Fig. 8). Since filtering has the effect of smoothing out spikes and lowering peak amplitudes, we here use raw data (black). Curve fits are shown in green (the Aging Law) and red (the Slip Law). The parameters so determined are provided in Table 2. As shown in Fig. 7, both laws do a good job of fitting the steady-state friction (the y-intercept), the stiffness (the upslope of the peak), and $a$ and $b$. The only apparent difference is that the Slip law consistently provides a larger $D_c$ value than the Aging law (Fig. 7h). There is no significant dependence of $D_c$ on temperature or normal stress. Values for stiffness $k$ (kPa/μm) as measured from the slope of initial ramps (gray circles) and fit from the velocity step program are shown in Fig. 7i. The fit values (measured at the up step during the middle of the experiment) are consistently stiffer than the ramp in values. No apparent temperature dependence was observed in either measurement of *k*. A plot of (*a-b*) vs. temperature is shown in Fig. 8; at all temperatures and normal stresses from the study, the velocity step analysis shows (*a-b*) values that are velocity-strengthening.

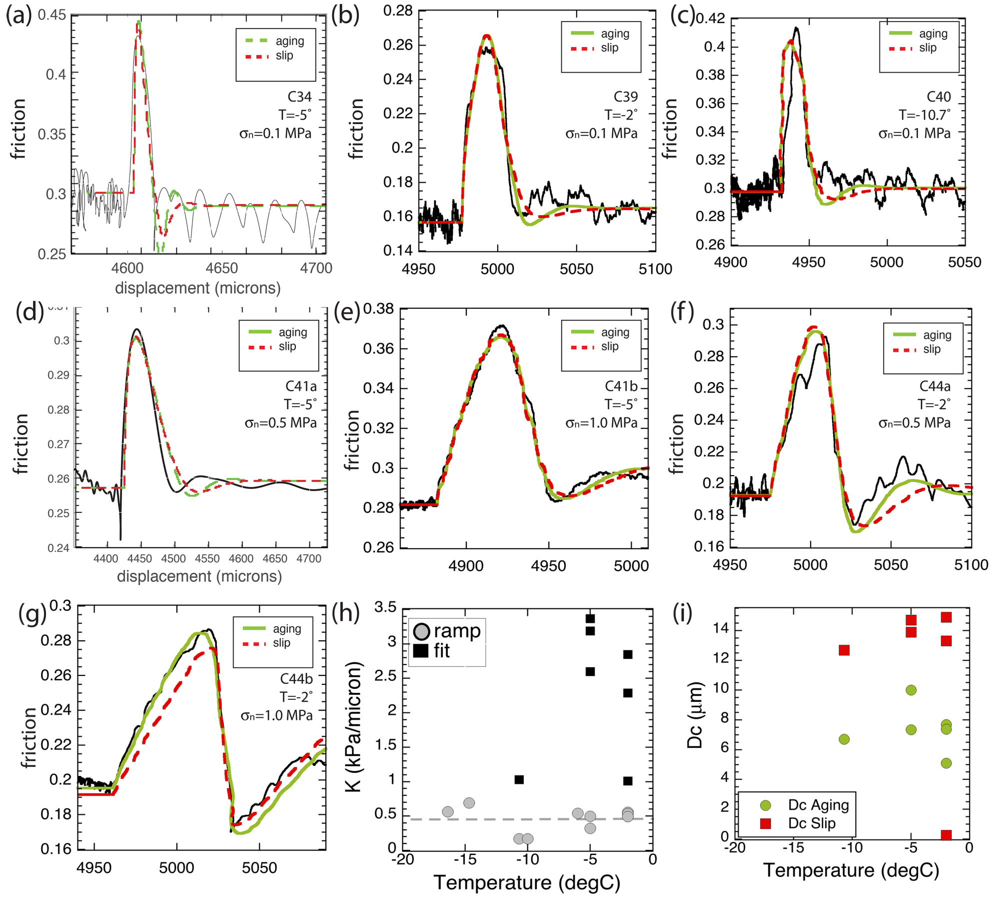


**Figure 7:** velocity up steps from 1 to 10 microns/s from experiments C34-44 with curve fits (of both Aging and Slip laws) overlain. (h) fitted values of $k$ from velocity steps and from the loading ramp as a function of temperature (at 0.1 MPa normal stress) and (i) $D_c$ (from Aging and Slip fits) as a function of temperature.

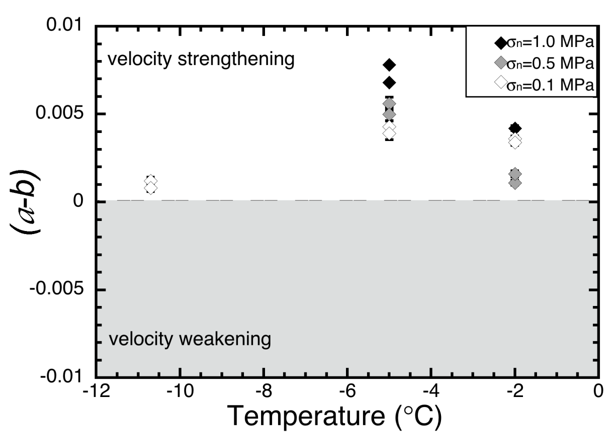

**Figure 8:** Rate dependence of friction, a-b, versus temperature, each measured from a velocity step from 1 µm/s to 10 µm/s using the GUI described in *Skarbek and Savage, 2019*. Where error bars cannot be seen, they are smaller than the symbol size. Analysis of velocity steps indicates only velocity strengthening behavior over this temperature/velocity range.

## 4.5 Reproducibility

Although not every set of conditions was reproduced, select temperatures and runs were performed in duplicate to test the reproducibility of the response. An example and discussion of this is provided in the Supplementary Material.

## 4.6 Forward Model results

In Fig. 9, we show forward modeling results of a slider block with measured RSF parameters (Table 2) with a sinusoidal load point velocity (Eq. 1) at applicable periods and amplitudes, compared to the measured experimental response from three runs, which were selected for their variations in temperature and normal stress. The values used in the forward model were those determined from Slip fits to velocity steps (Table 2). In all three figures, we see that the model predicts, with only small differences, the variations in frictional response. One significant deviation occurs in the far left of each figure. Just prior to the high frequency oscillations was a down step in median velocity from the 10 µm/s ramp to 1 µm/s branch of the run (Fig. 1). The overall experimental response to the down velocity step is a direct drop and gradual evolution to new background state, with the oscillations superimposed. These down step conditions were not incorporated into the forward model. The predictions are striking in their ability to capture both form and amplitude. Since the model does not include inertia, it does not predict the large high frequency stick-slips, with stress drops. In order for the model to predict such behavior, a model with inertia must be included [e.g., *Im et al*., 2017].

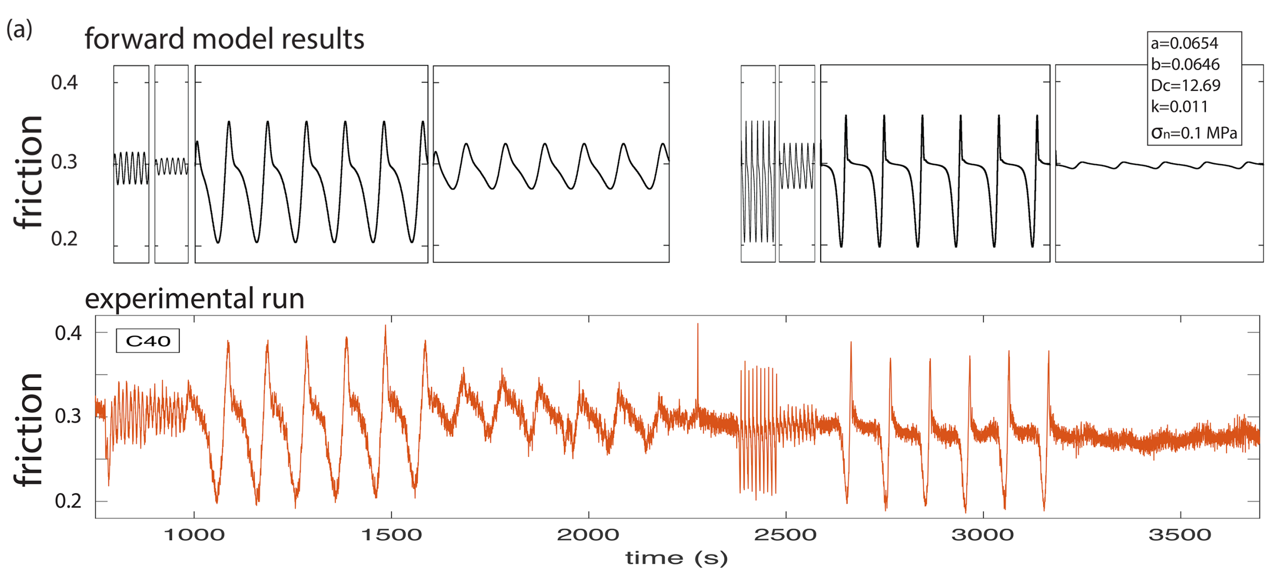

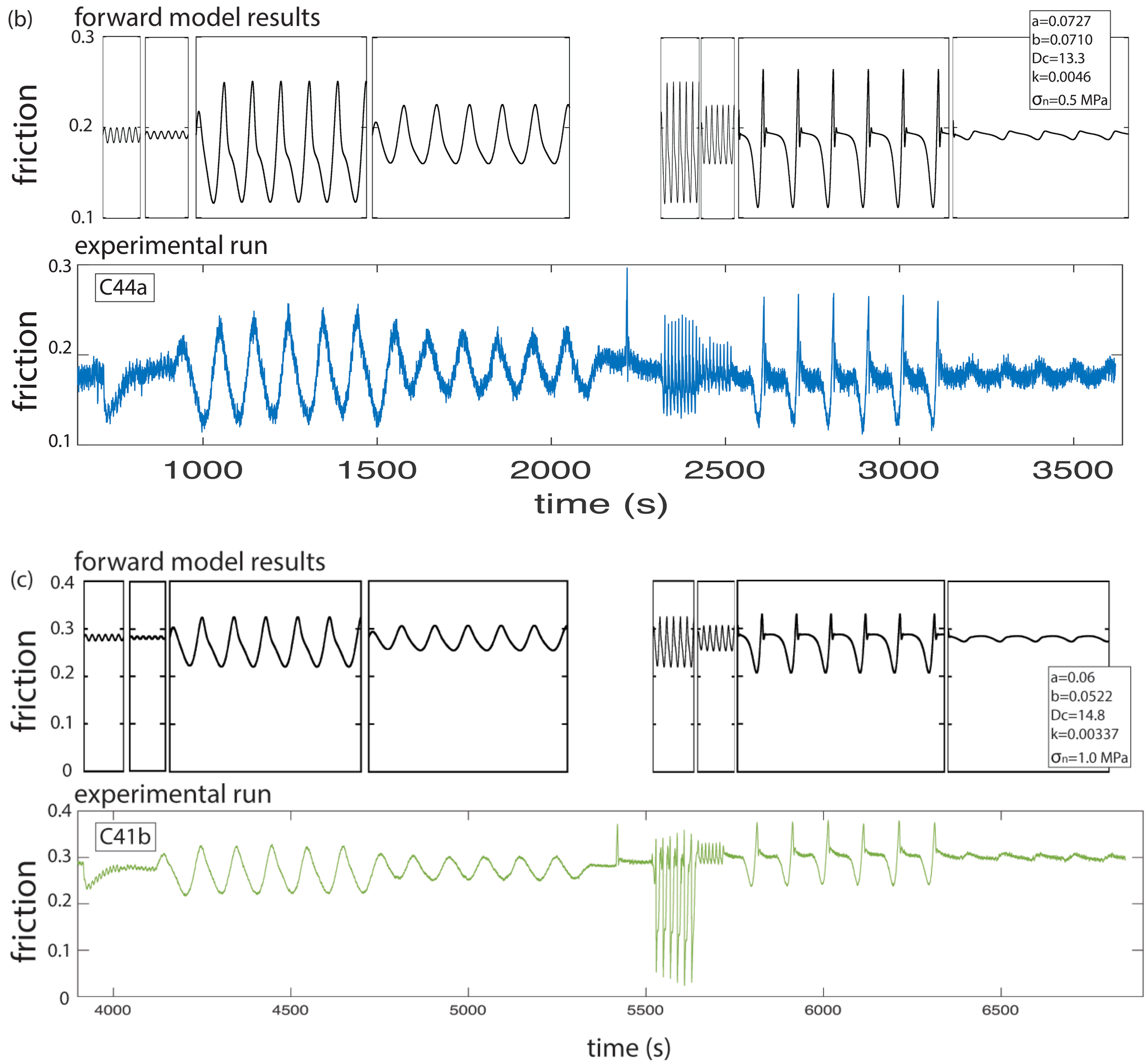


**Figure 9:** Forward model results compared to three selected experimental runs. Values for models are those listed, which are determined from the velocity step analysis (Table 2) using the Slip form of state. (a) at normal stress = 100 kPa; (b) at a mid-range of normal stress = 500 kPa; and (c) at highest normal stress = 1000 kPa.

## 5. Discussion

In these experiments, we see that oscillatory modulation of frictional sliding depends on a combination of amplitude and frequency of the load velocity, normal stress, and stiffness of the system. Temperature and median velocity play only a minor role. We categorize the responses into four groups: no modulation, smooth modulation, slow-slip events (which are ostensibly relaxation holds superimposed on a sine wave), and stick-slips. No measurable change in frictional sliding is found for conditions of low normal stress (100 kPa) with low amplitude (less than 50% of $V_m$) and long period (100 s). We interpret this to mean that the stressing rate is slow enough throughout the modulation to not perturb the average friction. At higher normal stresses and smaller amplitudes, we see smooth modulation. At longer periods and high amplitudes, healing is activated and slow-slip events occur. As indicated by the dashed lines in Fig. 1b, the amplitude of the frictional response at $V_m$ = 1 μm/s and $V_m$ = 10 μm/s are nearly the same ($\Delta\mu \sim 0.125$) when the amplitude of the forcing velocity is 100% of $V_m$. This demonstrates that the amplitude of the frictional response is not proportional to the oscillation amplitude of the driving velocity, but rather the ratio of the oscillation amplitude to the median driving velocity and in particular is sensitive to whether the velocity approached or equaled zero, as is the case during a hold.

We emphasize that a full spectrum of slip responses, from steady sliding to stick-slip, can be generated by small changes in our driving conditions. However, fitting to the velocity steps in our experiments show that the frictional rate parameters are velocity strengthening for all conditions tested here. Although we did not test a wide range of conditions, previous work has shown that ice friction analyzed in this way is generally velocity strengthening at a wide range of velocities at temperature above -12°C [*McCarthy et al., 2017; Zoet et al., 2013*]. In a companion paper, however, fitting to the oscillations directly produced dominantly velocity-weakening behavior [*Skarbek et al, 2021*].

Although *a-b* values are slightly positive and within a range commonly seen in friction experiments, the absolute values of *a* and *b* are large compared to most studies of rock at lower homologous temperature. These high values may be in part due to high healing. In our previous study [*McCarthy et al.*, 2017], we demonstrated through slide-hold-slide experiments that ice exhibits strong healing during holds. Healing is typically described in the rock mechanics literature as $\beta = \Delta\mu$ /log (time). The measured healing ($\beta$) of ice on rock from our previous study was at least an order of magnitude greater than that of rocks despite showing comparable steady-state friction values. Similar high healing was observed in other ice on rock and ice on till friction studies [*Zoet et al*. 2013; *Zoet and Iverson*, 2018]. Due to the high homologous temperature of ice at these conditions (which are consistent with terrestrial glaciers and ice streams) healing has been attributed to changes in real area of contact accomplished by high temperature viscous deformation [*Kennedy et al.,* 2000; *Schulson and Fortt*, 2012; and *McCarthy et al.,* 2017] and pressure-enhanced melting at asperities [*Zoet and Iverson*, 2018].

Although laboratory healing rates for ice are much higher than for rock, fault sliding behavior may be similarly dictated by healing rates. Faults have been shown to be sensitive to oscillating stresses at a variety of frequencies, such as seismic waves, tidal stresses, and seasonal loading due to snowpack, groundwater and surface water fluctuations [*Hill et al.,* 1993; *Gomberg et al*., 2001; *Heki*, 2003; *Saar and Manga*, 2003; *Cochran et al.,* 2004; *Brodsky and Prejean*, 2006; *Johnson et al.,* 2017]. Faults like the San Andreas have shown that low-frequency earthquakes and tremor are sensitive to tides in its creeping section [e.g., *Thomas et al,* 2009; *van der Elst et al*, 2016]. These events are mostly located below 20 km and might be enhanced by higher healing rates at relatively higher homologous temperatures than more shallow portions of the fault. We suggest that more experiments at high homologous temperatures for common fault rocks might further demonstrate the influence that enhanced fault healing at high temperatures might influence on fault slip style towards the brittle/ductile transition and below.

We postulate that the frictional response of ice can be thought of as a competition between stressing rate and healing rate. When strain rate is modest compared to healing rate, little healing occurs, and the sliding follows the forcing oscillation. When stressing rate is low, for instance at longer periods during the approach to zero velocity, frictional healing has more time to be effective, and healing-induced slow slip events occur. Only at the highest stressing rates do we see true stick-slip events. These occur when the normal stress is high and the velocity is increasing at higher rate (i.e. where the peak acceleration $\dot{V}$ is high, not peak velocity, which is the same for almost all experiments: ~20 μm/s), which is why stick-slip events are seen in the 10 s periods but rarely in the 100 s periods. Figure 10 is a response "phase diagram" which qualitatively maps out the style of sliding (for the four types defined at the beginning of this section) in stress vs. strain rate space. More specifically we plot the change in friction normalized by steady state friction (to remove temperature dependence) multiplied by normal stress versus forcing period, $\sigma_n/\dot{\tau}$, where stressing rate $\dot{\tau}$ equals $k^*\dot{V}/Vm$.

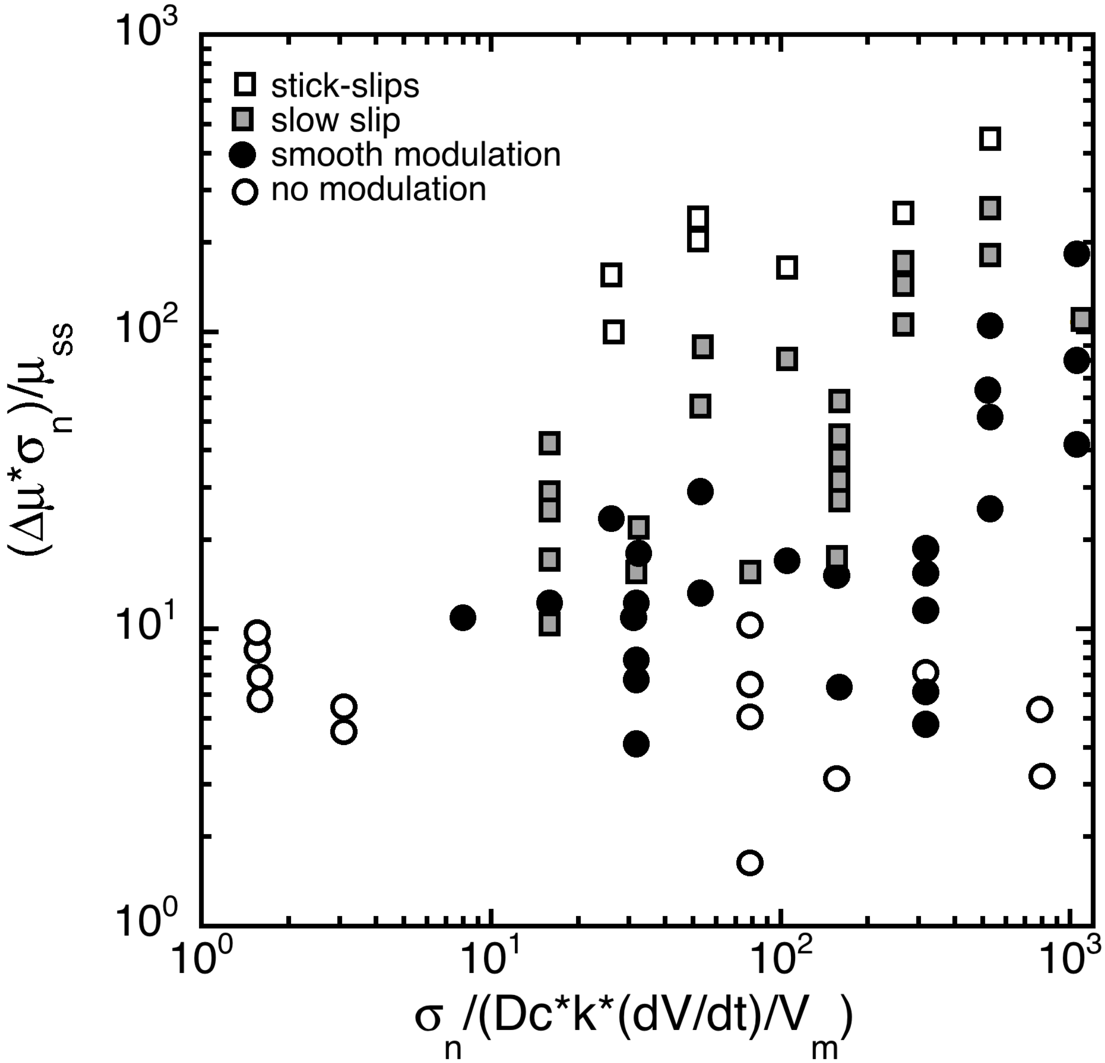


**Figure 10:** Simple response phase diagram demonstrating the effect of stressing rate on the frictional response style and amplitude (normalized delta friction times normal stress).

At almost all conditions, forward modeling with a simple 1D slider, a periodic forcing velocity, and rate-state parameters determined from velocity steps can predict the frictional response. However, the high stressing rate experiments, which cause stick-slips and large stress drops, cannot be predicted by the simple model. In a companion paper, *Skarbek et al.,* 2021, we determine the rate-state parameters directly from oscillatory data, instead of velocity steps. In such analysis, velocity-weakening parameters were measured from these same experiments. Previous studies have demonstrated that rate dependence can depend on velocity [*Ikari and Saffer*, 2011], so it should come as no surprise that a system with ever changing velocity may have different frictional properties than those measured at steady state. The new method of determining parameters from oscillatory data not only allows for significantly more information to be pulled from an experiment such as ours, it also provides a means of determining rate-state parameters from naturally oscillating systems.

### 4.7 Implications for ice sheets and glaciers

Sliding under ice sheets and glaciers should be controlled by a similar competition between healing and strain rate. Assuming that the bases of glaciers are near the pressure melting point and experience low effective normal stress, we would assume that variations in frictional sliding behavior emerges from a difference in velocity induced by the tides. Taking the assumptions provided by *Winberry et al, 2009*, the water height can be described as a resistive force to constant upstream force, such that the net force is sinusoidal. When the tide is high, the resistance is high and velocity slows; when tide is low, resistance is low and velocity increases. The amplitudes in downstream velocity thus depend on local conditions. In places with a low median sliding rate compared to tidal amplitude, our experimental results suggest that these locations would be likely to experience significant healing during their cycle. In places additionally having localized high normal stress, we would expect unsteady sliding, as seen at Whillans Ice Stream. Although there are length and time scaling differences between our lab experiments and nature, we achieve similar normal stress, temperature, and median sliding rate conditions. Estimates of stress accumulation over recurrence time for Whillans yield a healing rate of 0.029/log(s) [*Winberry et al.* 2009, 2014]. At temperatures greater than -5°C, this is in line with our lab estimates of healing at 100 kPa normal stress. The similarities in healing rate are somewhat surprising, as our sample configuration of ice on rock is quite simplistic compared to the ice-till-bedrock interface beneath glaciers. That the timing of events in our experiments (just before peak velocity and just after low velocity) correspond to events timed just before low tide and just after high tide is additionally intriguing.

One important difference between our laboratory conditions and natural conditions is that the period of our forcing signal (1 – 100 s) is orders of magnitude shorter than the period of the diurnal tide experienced by many ice sheets (~$10^4$ s). If the response to different periods is a function of $D_c$, we can estimate the $D_c$ for ice streams based on the ratio of $D_c/P$ of our experiments. We see the most stick-slip behavior at 10 s periods, and our average $D_c$ is ~10 μm. The tides at Whillans are 24-hour diurnal tides (86,400 s), so to scale up our experimental results would require a $D_c$ of ~86 mm. As the base of the ice sheet should contain a much wider range of asperity sizes, the critical displacement length should also scale and our estimate of tens of mm is in order of magnitude agreement with frictional modeling studies of Whillans Ice Stream [*Lipovskly and Dunham*, 2017].

## 5 Conclusions

The results from this study show that rate and state dependent friction formulations can describe oscillatory frictional behavior in ice. The Aging and Slip forms of state appear to be equally suitable to describing the velocity steps in this study. The ability of small variations in velocity to create large variations in the frictional response is likely due to high healing at the ice-rock interfaces, which at this high homologous temperature, is orders of magnitude greater than healing values measured in low temperature studies of rocks. Both the experimental work of ice on rock here (which replicates most of the conditions of ice streams) and natural ice streams are more influenced by the tides than their land-based, rocky brethren [e.g. *Vidale et al.,* 1998]. Although analysis of velocity steps shows velocity-strengthening behavior at all conditions tested here, distinct repeatable stick-slips were observed at some conditions. A companion paper [*Skarbek et al*., 2021] provides a way of analyzing oscillatory data directly, and in so doing, determined velocity-weakening behavior.

**Table 1:** List of experiments, intended driving conditions*, and measured steady state friction and run-in stiffness (determined from the loading ramp at the beginning of experiments). *Fitted velocities were 1.1 and 11.1 μm/s.

| Exp# | Temp (°C) | Background $V_m$ (μm/s) | Frequency (Hz) | Amplitudes (μm/s) | Normal stress (MPa) | $\mu_{SS}$ | *k* Ramp kPa/$\mu m$ |
|---|---|---|---|---|---|---|---|
| C29 | -14.7 | 10 | 1, 0.1, 0.01 | 10, 5, 2 | 0.1 | 0.39 | 0.693 |
| C30 | -10 | 10 | 1, 0.1, 0.01 | 10, 5, 2 | 0.1 | 0.29 | 0.170 |
| C31 | -6 | 10 | 1, 0.1, 0.2, 0.01, 0.02 | 10, 5, 2 | 0.1 | 0.27 | 0.541 |
| C32 | -2 | 10 | 1, 0.1, 0.01 | 10, 5, 2 | 0.1 | 0.19 | 0.636 |
| C33 | -16.4 | 10 | 1, 0.1, 0.2, 0.01, 0.02 | 10, 5, 2 | 0.1 | 0.33 | 0.562 |
| C34 | -5 | 1, 10 | 0.1, 0.01 | 10, 5 | 0.1 | 0.28 | 0.324 |
| C39 | -2 | 1, 10 | 0.1, 0.01 | 10, 5 | 0.1 | 0.15 | 0.556 |
| C40 | -10.7 | 1, 10 | 0.1, 0.01 | 10, 5 | 0.1 | 0.29 | 0.171 |
| C41 | -5 | 1, 10 | 0.1, 0.01 | 10, 5 | 0.5<br>1.0 | 0.28 | a0.498<br>b |
| C44 | -2 | 1, 10 | 0.1, 0.01 | 10, 5 | 0.5<br>1.0 | 0.18 | a0.537<br>b0.495 |

**Table 2:** fitted rate-state parameters to velocity up steps in Fig. 6

| Fig | # | T (°C) | $\sigma_n$ MPa | $\mu_{ss}$ | *a* | *b* | $D_c$ $\mu m$ | $K^*$ $kPa/\mu m$ | *(a-b)* *[std dev]* | Law |
|---|---|---|---|---|---|---|---|---|---|---|
| a | C34 | -5 | 0.1 | 0.292 | 0.0946 | 0.0903 | 3.30 | 0.03 | 0.0043 | aging |
| | | | | 0.292 | 0.0946 | 0.0907 | 6.26 | 0.03 | 0.0039 | slip |
| b | C39 | -2 | 0.1 | 0.157 | 0.0667 | 0.0630 | 7.69 | 1.01 | 0.0036 [$1.6\times10^{-4}$] | aging |
| | | | | 0.157 | 0.0652 | 0.0618 | 14.9 | 1.01 | 0.0034 [$1.7\times10^{-4}$] | slip |
| c | C40 | -10.7 | 0.1 | 0.298 | 0.0661 | 0.0649 | 6.7 | 1.03 | 0.0012 [$2.1\times10^{-4}$] | aging |
| | | | | 0.298 | 0.0654 | 0.0646 | 12.69 | 1.03 | 0.0008 [$2.1\times10^{-4}$] | slip |
| d | C41a | -5 | 0.5 | 0.252 | 0.0565 | 0.0509 | 7.35 | 3.19 | 0.0056 [$3.7\times10^{-4}$] | aging |
| | | | | 0.252 | 0.0551 | 0.0501 | 13.9 | 3.14 | 0.0050 [$3.7\times10^{-4}$] | slip |
| e | C41b | -5 | 1.0 | 0.282 | 0.0578 | 0.0510 | 10 | 3.37 | 0.0068 [$6.2\times10^{-5}$] | aging |
| | | | | 0.282 | 0.0600 | 0.0522 | 14.8 | 3.37 | 0.0078 [$7.2\times10^{-5}$] | slip |
| f | C44a | -2 | 0.5 | 0.193 | 0.0731 | 0.0720 | 7.38 | 2.85 | 0.0011 [$1.4\times10^{-4}$] | aging |
| | | | | 0.192 | 0.0727 | 0.0710 | 13.3 | 3.0 | 0.0016 [$1.7\times10^{-4}$] | slip |
| g | C44b | -2 | 1.0 | 0.195 | 0.098 | 0.0939 | 5.09 | 2.29 | 0.0042 | aging |

| | | | | | | | | | | |
|---|---|---|---|---|---|---|---|---|---|---|
| | | | | | | | | | [$1.4\times10^{-4}$] | |
| | | | | 0.192 | 1.1771 | 1.1701 | 0.25 | 1.79 | 0.0034 [$1.7\times10^{-4}$] | slip |

## 6 Conflict of Interest

*The authors declare that the research was conducted in the absence of any commercial or financial relationships that could be construed as a potential conflict of interest.*

## 7 Author Contributions

C.M. ran experiments, analysed the data, and initiated publication. R.S. wrote the programs for determining rate-state parameters from velocity steps and the forward modelling routine and assisted with writing and interpretation of results. H.S. advised on experimental methods, interpretation of results, and writing of publication.

## 8 Funding

The study was funded by NSF under award no. ANT 1245871.

## 9 Acknowledgments

The authors wish to thank ____.

## 10 Data Availability Statement

The datasets generated by this study can be downloaded from USAP-DC at https://doi.org/10.15784/601497.

## References

Anandakrishnan, S. and R. B. Alley (1997). Tidal forcing of basal seismicity of Ice Stream C, West Antarctica, observed far inland. J. Geophys. Res. 102, 15,183-15,196.

Anandakrishnan, S., D. E. Voigt, R. B. Alley, M. A. King (2003). Ice stream D flow speed is strongly modulated by the tide beneath the Ross Ice Shelf. Geophys. Res. Letters 30:7, 1361.

Bamber, J. L., D. G. Vaughan, and I. Joughin (2000). Widespread Complex Flow in the Interior of the Antarctic Ice Sheet. Science 287(5456), 1248-1250.

Barcheck, G., Brodsky, E. E., Fulton, P. M., King, M. A., Siegfried, M. R., & Tulaczyk, S. (2021). Migratory earthquake precursors are dominant on an ice stream fault. Science Advances, 7(6), eabd0105.

Beeler, N.M. and D.A. Lockner (2003). Why earthquakes correlate weakly with the solid Earth tides: Effects of periodic stress on the rate and probability of earthquake occurrence. J. Geophys. Res. 108:B8, 2391.

Bhattacharya, P., Rubin, A.M., Bayart, E., Savage, H.M., and Marone, C. (2015). Critical evaluation of state evolution laws in rate and state friction: Fitting large velocity steps in simulated fault gouge with time-, slip-, and stress-dependent constitutive laws. J. Geophys. Res.: Solid Earth, 120, 6365–6385.

Bhattacharya, P., Rubin, A.M., and Beeler, N.M. (2017). Does fault strengthening in laboratory rock friction experiments really depend primarily upon time and not slip? J. Geophys. Res.: Solid Earth, 122, 6389–6430.

Bindschadler, R. A., M. A. King, R. B. Alley, S. Anandakrishnan, and L. Padman (2003). Tidally controlled stick-slip discharge of a West Antarctic Ice Stream. Science 301, 1087-1089.

Bindschadler, R., P. Vornberger, M. King, and L. Padman (2002). Tidally-driven stick-slip motion in the mouth of Whillans Ice Stream, Antarctica. Annals of Glaciology *36:1, 263-272.*

Blanpied, M. L., T. E. Tullis, J. D. Weeks (1998). Effects of slip, slip rate, and shear heating on the friction of granite. J. Geophys. Res. 103(B1), 489-511.

Boettcher, M.S. and C. Marone (2004). Effects of normal stress variation on the strength and stability of creeping faults. J. Geophys. Res. 109 (B03406).

Brodsky, E. E., & Prejean, S. G. (2005). New constraints on mechanisms of remotely triggered seismicity at Long Valley Caldera. J. Geophys. Res.: Solid Earth 110(B4).

Brunt, K.M., M.A. King, H.A. Fricker, and D.R. MacAyeal (2010). Flow of the Ross Ice Shelf, Antarctica, is modulated by the ocean tide. J. Glaciology 56:195, 157-161.

Brunt, K. M. and D. R. MacAyeal (2014). Tidal modulation of ice-shelf flow: a viscous model of the Ross Ice Shelf, J. Glaciology 60:221, 500-508.

Carpenter, B. M., C. Marone, and D. M. Saffer (2011). Weakness of the San Andreas Fault revealed by samples from the active fault zone. Nature Geoscience 4, 251-254.

Clarke, G. K.C. (2005). Subglacial Processes, Ann. Rev. Earth Planet. Sci. 33:247-76.

Cochran, E. S., Vidale, J. E., & Tanaka, S. (2004). Earth tides can trigger shallow thrust fault earthquakes. Science 306(5699), 1164-1166

Cole, D. M. (1979). Preparation of polycrystalline ice specimens for laboratory experiments. Cold. Reg. Sci. Tech.1, 153-159.

Dieterich, J. H. (1978). Time-dependent friction and the mechanics of stick-slip. Pure Appl. Geophys. 116, 790-806.

Dieterich, J. H. (1979). Modeling of rock friction: 1. Experimental results and constitutive equations. J. Geophys. Res. Solid Earth 84:B5, 2161-2168.

Dieterich, J. H. (1981). Constitutive properties of faults with simulated gouge, in Mechanical Behavior of Crustal Rocks, Geophys. Monogr. Ser., vol. 24, edited by N. L. Carter, M. Friedman, J. M. Logan, and D. W. Stearns, 103-120, AGU, Washington, D.C.

Dieterich, J. H. (1994). A constitutive law for rate of earthquake production and its application to earthquake clustering. J. Geophys. Res., 89(B6), 4196-4202.

Doake, C.S. M., H.F.J. Corr, K.W. Nicholls, A. Gaffikin, A. Jenkins, W.I. Bertiger, and M.A. King (2002). Tide-induced lateral movement of Brunt Ice Shelf, Antarctica. Geophys. Res. Lett. 28:0, 1226.

Gomberg, J., Reasenberg, P. A., Bodin, P. L., & Harris, R. A. (2001). Earthquake triggering by seismic waves following the Landers and Hector Mine earthquakes. Nature, 411(6836), 462-466

Gudmundsson, G. H. (2007) Tides and the flow of Rutford Ice Stream, West Antarctica, J. Geophys. Res.- Earth Surface, 112, F04007.

Heki, K. (2003). Snow load and seasonal variation of earthquake occurrence in Japan. Earth and Planetary Science Letters, 207(1-4), 159-164.

Hill, D. P., Reasenberg, P. A., Michael, A., Arabaz, W. J., Beroza, G., Brumbaugh, D., ... & Zollweg, J. 1. (1993). Seismicity remotely triggered by the magnitude 7.3 Landers, California, earthquake. Science, 260(5114), 1617-1623

Hong, T. and C. Marone (2005). Effects of normal stress perturbations on the frictional properties of simulated faults, Geochem., Geophys. Geosyst. 6:Q03012.

Ikari, M. J., & Saffer, D. M. (2011). Comparison of frictional strength and velocity dependence between fault *zones* in the Nankai accretionary complex. Geochemistry, Geophysics, Geosystems, 12(4).

Im, K., D. Elsworth, C. Marone, and J. Leeman (2007) The impact of frictional healing on stic-slip recurrence interval and stress drop; Implications for earthquake scaling. J. Geophys. Res.: Solid Earth 122, 10,102-10,117.

Johnson, C. W., Fu, Y., & Bürgmann, R. (2017). Seasonal water storage, stress modulation, and California seismicity. Science, 356(6343), 1161-1164.

Kennedy, F. E., E.M. Schulson, and D.E. Jones (2000). The friction of ice on ice at low sliding velocities. Philos. Mag. A. 80, 1093-1110.

Lipovsky, B. P., and E. M. Dunham (2017). Slow-slip events on the Whillans Ice Plain, Antarctica, described using rate-and-state friction as an ice stream sliding law, J. Geophys. Res.: Earth Surface 122, 973-1003.

Lipovsky, B. P., C. R. Meyer, L. K. Zoet, C. McCarthy, D. D. Hansen, A. W. Rempel, and F. Gimbert (2019). Glacier sliding, seismicity and sediment entrainment, Annals of Glaciology 60(79), 182- 192.

Lockner, D. A. and N. M. Beeler (1995). Premonitory slip and tidal triggering of earthquakes, J. Geophys. Res. 104(B9), 20,133-20,151.

Makinson, K., M.A. King, K.W. Nicholls, and G. H. Gudmundsson (2012). Diurnal and semidiurnal tide-induced lateral movement of Ronne Ice Shelf, Antarctica, Geophys. Res. Lett., 39, L10501.

Marone, C. (1998). Laboratory-derived friction laws and their application to seismic faulting, Annual Review of Earth and Planetary Sciences 26, 643-696.

McCarthy, C., H. Savage, T. Koczynski, and M. Nielson (2016). An apparatus to measure frictional, anelastic, and viscous behavior in ice at temperate and planetary conditions, Rev. Sci. Inst. *87, 055112.*

McCarthy, C., H. Savage, and M. Nettles (2017). Temperature dependence of ice-on-rock friction at realistic glacier conditions, Philosophical Transactions of the Royal Society A, *375(2086),* 20150348.

Minchew, B. M., M. Simons, B. Riel and P. Milillo (2017). Tidally induced variations in vertical and horizontal motion on Rutford Ice Stream, West Antarctica, inferred from remotely sensed observations. J. Geophys. Res.: Earth Surface, 122, 167-190.

Murray, T., A. M. Smith, M. A. King, G. P. Weedon (2007). Ice flow modulated by tides at up to annual periods at Rutford Ice Stream, West Antarctica. Geophys. Res. Lett. 34(18), L18503.

Perfettini, H. and J. Schmittbuhl (2001). Periodic Loading on a creeping fault: Implication for Tides. Geophys. Res. Lett. 28:3, 435-438.

Perfettini, H., J. Schmittbuhl, and A. Cochard (2003). Shear and normal load perturbations on a two-dimensional continuous fault: 1. Static triggering, J. Geophys. Res. 108: B9, 2409.

Pratt, M.J., J.P. Winberry, D.A. Wiens, S. Anandakrishnan, and R.B. Alley (2014). Seismic and geodetic evidence for grounding-line control of Whillans Ice Stream stick-slip events. J. Geophys. Res. Earth Science, 119, 333-348.

Reinan, L. A. and J. D. Weeks (1993). Determination of rock friction constitutive parameters using an iterative least-squares inversion method. J. Geophys. Res. 98, 15,937-15,950.

Rice, J.R. and A.L. Ruina (1983). Stability of Steady Frictional Slipping, J. Appl. Mech. 50(2), 343-349.

Richardson, E. and C. Marone (1999). Effects of normal stress vibrations on frictional healing, J. Geophys. Res. 104:B12, 28,859-28,878.

Riedel, B. Nixdorf, U., Heinert, M., Eckstaller, A. and Mayer, C. (1999). The response of the Ekströmisen (Antarctica) grounding zone to tidal forcing. *Annals of Glaciology*, 29, 239-242.

Rosier, S. H. R., G. H. Gudmundsson, and J. A. M. Green (2014). Insights into ice stream dynamics through modeling their response to tidal forcing, *The Cryosphere*, 8, 1763-1775.

Rosier, S. H. R., G. H. Gudmundsson, M.A. King, K. W. Nicholls, K. Makinson, and HFJ. Corr (2017). Strong tidal variations in ice flow observed across the entire Ronne Ice Shelf and adjoining ice streams. Earth Syst. Sci. Data, 9, 849-860.

Ruina, A. (1983). Slip Instability and State Variable Friction Laws, J. Geophys. Res. 88, B12, 10,359-10,370.

Saar, M. O., & Manga, M. (2003). Seismicity induced by seasonal groundwater recharge at Mt. Hood, Oregon. Earth and Planetary Science Letters, 214(3-4), 605-618.

Savage, H. M. and C. Marone (2007). Effects of shear velocity oscillations on stick-slip behavior in laboratory experiments. J. Geophys. Res. 112: B02301.

Savage, H.M. and C. Marone (2008). The potential for earthquake triggering from transient deformations, J. Geophys. Res 113, B05302, doi:10.1029/2007JB005277.

Scholz, C. H. (2002). The mechanics of earthquakes and faulting, 2nd edn., New York, NY: Cambridge University Press.

Schulson, E. M. and A. L. Fort (2012). Friction of ice on ice. J. Geophys. Res. 117, B12204.

Skarbek, R. M. and H. M. Savage (2019). RSFit3000: A MATLAB GUI-based program for determining rate and state frictional parameters from experimental data, *Geosphere*, 15:5, 1665-1676.

Skarbek, R. M., C. McCarthy, and H. M. Savage (2021). Oscillatory loading can alter the velocity rate dependence of ice-on-rock friction. To be submitted to *Geochemistry, Geophysics, and Geosystems.*

Thomas, A. M., R. M. Nadeau, and R. Burgmann (2009). Tremor-tide correlations and near-lithostatic pore pressure on the deep San Andreas fault. Nature 462(7276), 1048-1051.

Tworzydlo, W. W. and O. N. Hamzeh (1997). On the importance of normal vibrations in modeling of stick-slip in rock sliding. J. Geophys. Res., Solid Earth, 102:B7, 15,091-15,103.

van der Elst, N.J. and H. M. Savage (2015). Frequency dependence of delayed and instantaneous triggering on laboratory and simulated faults governed by rate-state friction. J. Geophys. Res. Solid Earth 120(5), 3406-3429.

van der Elst, N. J, A. A. Delorey, D. R. Shelly, and P. A. Johnson (2016). Fortnightly modulation of San Andreas tremor and low-frequency earthquakes, Proc. Nat. Acad. Sciences 113(31) 8601-8605.

Vidale, J. E., D. C. Agnew, M. J. S. Johnston, D. H. Oppenheimer (1998). Absence of earthquake correlation with Earth tides: An indication of high preseismic fault stress rate. J. Geophys. Res. Solid Earth 103(B10), 24,567-24,572.

Voisin, C. (2001). Dynamic triggering of earthquakes: The linear slip-dependent friction case. Geophys. Res. Lett. 28, 3357-3360.

Voisin, C. (2002) Dynamic triggering of earthquakes: The nonlinear slip-dependent friction case. J. Geophys. Res. Solid Earth 107 (B12), ESE 10-1-ESE 10-11.

Wiens, D. A., S. Anandakishnan, J.P. Winberry, and M.A. King (2008). Simultaneous teleseismic and geodetic observations of the stick-slip motion of an Antarctic ice stream. Nature Letters 453, 770-775.

Winberry, J.P., S. Anandakishnan, R.B. Alley, R.A. Bindschadler, and M.A. King (2009). Basal mechanics of ice streams: Insights from the stick-slip motion of Whillans Ice Stream, West Antarctic. J. Geophys. Res. 114, F01016

Winberry, J.P., S. Anandakrishnan, D.A. Wiens, R. B. Alley, and K. Christianson (2011). Dynamics of stick-slip motion, Whillans Ice Stream, Antarctica. Earth Planet. Lett. 305, 283-289.

Winberry, J. P., S. Anandakrishnan, R. B. Alley, D. A. WIends, adn M. J. Pratt (2014). Tidal pacing, skipped slips and the slowdown of Whillans Ice Stream, Antarctica. Journal of Glaciology 60, 795-807.

Wuite, J., K.C. Jezek, X. Wu, K. Farness, and R. Carande (2009). The velocity field and flow regime of David Glacier and Dryglaski Ice Tongue, Antarctica. Polar. Geography 32(3-4), 111-127.

Zoet, L.K., B. Carpenter, M. Scuderi, R.B. Alley, S. Anandakrishnan, C. Marone, and M. Jackson (2013). The effects of entrained debris on the basal sliding stability of a glacier. J. Geophys. Res.: Earth Surface, 118, 656-666.

Zoet, L.K. and N. R. Iverson (2018). A healing mechanism for stick-slip of glaciers. Geology 46: 9, 807-810.